Ground-state Dirac monopole

E. Ruokokoski,[1] V. Pietilä,[2] and M. Möttönen[1,3]
[1]*Department of Applied Physics/COMP, Aalto University, P.O. Box 14100, FI-00076 AALTO, Finland*
[2]*Physics Department, Harvard University, Cambridge, Massachusetts 02138, USA*
[3]*Low Temperature Laboratory, Aalto University, P.O. Box 13500, FI-00076 AALTO, Finland*
(Received 4 October 2011; published 21 December 2011)

We show theoretically that a monopole defect, analogous to the Dirac magnetic monopole, may exist as the ground state of a dilute spin-1 Bose-Einstein condensate. The ground-state monopole is not attached to a single semi-infinite Dirac string but forms a point where the circulation of a single vortex line is reversed. Furthermore, the three-dimensional dynamics of this monopole defect is studied after the magnetic field pinning the monopole is removed and the emergence of antimonopoles is observed. Our scheme is realizable with the current experimental facilities.

DOI: 10.1103/PhysRevA.84.063627 PACS number(s): 03.75.Mn, 03.75.Lm, 67.85.Fg

I. INTRODUCTION

Topologically nontrivial configurations of quantum and classical fields play a fundamental role in the physics of various phase transitions ranging from superfluids to the early universe [1,2]. In particular, they can give rise to exotic quantum states relevant to electromagnetism [3], elementary particles [4], grand unified theories [5], and cosmology [6]. Given the difficulties of making detailed observations on cosmological scales or probing conventional matter on ultrashort length scales, experimental evidence for many of these topological excitations is scarce and indirect at most.

Dilute ultracold Bose gases with a spin degree of freedom can host a variety of topologically interesting structures, such as coreless vortices, knotted textures, skyrmions, and several types of monopoles [7–15]. The high controllability of these quantum systems and their observability using optical imaging techniques allow, in principle, detailed experimental investigations of the various defects. In practice, topologically nontrivial configurations occur as excited states and their topological nature dictates that they cannot be easily created from a topologically trivial ground state. In particular, configurations relevant to tabletop experiments of exotic phenomena in high-energy physics and cosmology can be especially challenging to create in an atomic gas since they require intricate manipulation of the atomic cloud in all three spatial dimensions [16–20].

A major step forward was taken recently when a robust method for creating an analog of the Dirac monopole was proposed [20]. The Dirac monopole [3] is the simplest model for a magnetic point charge, which unlike its electric counterpart, has not been convincingly observed. In Ref. [20], the monopole defect was created into the spin texture of a dilute Bose–Einstein condensate (BEC) by adiabatically modifying external magnetic fields. The resulting monopole state is not the ground state of the system because of its tendency to degrade due to dynamical instabilities associated with the Dirac string. In this Article, we demonstrate that an analog of the Dirac monopole in an atomic gas can exist as a ground-state configuration. We find that in an experimentally feasible time-independent magnetic field the ground state of the BEC corresponds to a strong-field seeking state (SFSS) with a monopole defect. A similar defect is also found for the weak-field seeking state (WFSS). In contrast to the previous studies, we find that the minimum-energy monopole is not attached to a single Dirac string with two circulation quanta but is manifested as a point where the circulation of a single-quantum vortex is reversed. A similar configuration may be obtained from the ideal Dirac monopole by applying a gauge transformation [21]. Our results show that the Dirac monopole is a physically viable concept and can represent a robust and long-lived state.

We consider a condensate of ^{87}Rb atoms with ferromagnetic spin-spin interactions [22]. The total hyperfine spin of the constituent atoms is $F = 1$, and the order parameter is a three-component spinor field. In the presence of a strong external magnetic field, the condensate spin tends to align with the local field. Hence external fields can be used to imprint topologically nontrivial spin textures to the condensate. For topological reasons, the ferromagnetic phase cannot sustain stable isolated pointlike defects [23]. This does not, however, completely exclude the existence of point defects, as they may appear as endpoints of quantized vortices. These defects are characterized by a geometric charge Q_{3D} corresponding to the area on the unit sphere covered by the condensate spin as one encloses the point defect in the spatial coordinate space [20].

Let us consider an external magnetic field which is a combination of two crossing quadrupole fields,

$$\boldsymbol{B}(\boldsymbol{r}) = B_1'(x\hat{e}_x + y\hat{e}_y) + B_2' z\hat{e}_z. \tag{1}$$

Since $\boldsymbol{B}$ is a monopole-free field, Maxwell's equation $\nabla \cdot \boldsymbol{B} = 0$ imposes a condition $2B_1' + B_2' = 0$. The alignment of the hyperfine spin with the magnetic field in Eq. (1) gives rise to a spin texture that is depicted in Fig. 1(a) and has the geometric charge $Q_{3D} = 1$. The analogy to the Dirac monopole comes from the vorticity $\boldsymbol{\Omega}_s = \nabla \times \boldsymbol{v}_s$, where $\boldsymbol{v}_s$ is the superfluid velocity. The vorticity $\boldsymbol{\Omega}_s$ is equivalent to the magnetic field of a magnetic monopole and the Dirac monopole can be considered as a point source of the superfluid flow. Using the Mermin-Ho relation [24], the geometric charge Q_{3D} of the spin texture can be related to the total vorticity in the system. Vorticity corresponding to the spin texture in Fig. 1(a) takes almost everywhere the radially outward hedgehog form

$$\boldsymbol{\Omega}_s = \frac{\hbar}{mr'^2}\hat{\boldsymbol{e}}_{r'} \tag{2}$$

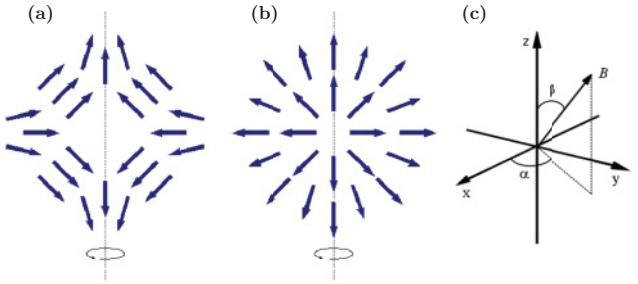

FIG. 1. (Color online) (a) Spin texture corresponding to the magnetic field in Eq. (1). (b) Vorticity $\boldsymbol{\Omega}_s$ corresponding to the spin texture in panel (a). Vector fields in panels (a) and (b) are symmetric with respect to rotations about the axis depicted with the dashed line. (c) Illustration of the polar angles α and β used to parametrize the local magnetic field $\boldsymbol{B}$.

in the scaled units $(x',y',z') = (x,y,2z)$ [20]. This establishes the analogy to the magnetic monopole proposed by Dirac [3].

II. MEAN-FIELD THEORY

In the zero-temperature limit, the stationary states of the condensate are solutions to the time-independent Gross–Pitaevskii (GP) equation [25],

$$\mathcal{H}[\Psi]\Psi(\boldsymbol{r}) = \mu\Psi(\boldsymbol{r}), \tag{3}$$

where the Hamiltonian for a spin-1 condensate is

$$\mathcal{H}[\Psi] = \hat{h}(\boldsymbol{r}) + c_0|\Psi(\boldsymbol{r})|^2 + c_2\Psi^\dagger(\boldsymbol{r})\boldsymbol{F}\Psi(\boldsymbol{r})\cdot\boldsymbol{F}. \tag{4}$$

Here, $\boldsymbol{\mathcal{F}} = (\mathcal{F}_x,\mathcal{F}_y,\mathcal{F}_z)^T$ is a vector of spin-1 matrices and $\hat{h}(\boldsymbol{r})$ is the single-particle Hamiltonian given by $\hat{h}(\boldsymbol{r}) = -\hbar^2\nabla^2/2m + V_{\rm opt}(\boldsymbol{r}) + g_F\mu_B\boldsymbol{B}(\boldsymbol{r})\cdot\boldsymbol{\mathcal{F}}$, where g_F is the Landé g-factor and μ_B is the Bohr magneton. Unless otherwise mentioned, we consider a three-dimensional optical trapping potential $V_{\rm opt}(\boldsymbol{r}) = m\omega_r^2r^2/2$. The coupling constants are given by $c_0 = 4\pi\hbar^2(a_0+2a_2)/3m$ and $c_2 = 4\pi\hbar^2(a_2-a_0)/3m$, where a_f is the s-wave scattering length corresponding to the channel with total hyperfine spin f. The Hamiltonian in Eq. (4) corresponds to a free-energy functional of the form [25,26]

$$E[\Psi] = \int d\boldsymbol{r}\left[\frac{\hbar^2}{2m}|\nabla\Psi(\boldsymbol{r})|^2 + [V_{\rm opt}(\boldsymbol{r})-\mu]|\Psi(\boldsymbol{r})|^2 + \frac{c_0}{2}|\Psi(\boldsymbol{r})|^4 + \frac{c_2}{2}|\boldsymbol{S}(\boldsymbol{r})|^2 + g_F\mu_B\boldsymbol{B}(\boldsymbol{r})\cdot\boldsymbol{S}(\boldsymbol{r})\right], \tag{5}$$

where $\boldsymbol{S} = \Psi^\dagger\boldsymbol{\mathcal{F}}\Psi$. The dynamics of the BEC is solved from the time-dependent GP equation, $i\hbar\partial_t\Psi = \mathcal{H}[\Psi]\Psi$, where $\mathcal{H}$ is given in Eq. (4).

Let us write the stationary order parameter in the form $\Psi = \varphi\boldsymbol{\zeta}$, where φ is a scalar field and $\boldsymbol{\zeta}$ is a spinor field normalized to unity. Assuming that the condensate spins align with the local field, the free energy of the system can be written as [27]

$$E[\Psi] = \int d\boldsymbol{r}\left\{\varphi^\dagger\left[\frac{1}{2m}(-i\hbar\nabla + m\boldsymbol{v}_s)^2 + g_F\mu_B B(\boldsymbol{r}) + \frac{\hbar^2}{2m}[|\nabla\zeta|^2 + (\zeta^\dagger\nabla\zeta)^2] + \mathcal{V}\varphi^\dagger\varphi\right]\varphi\right\}, \tag{6}$$

where $\mathcal{V}$ is the local interaction potential. Equation (6) is a Hamiltonian for a scalar particle with order parameter φ, and it is equivalent to the Hamiltonian for charged particles coupled to a vector potential $\boldsymbol{A}$. Hence the equation of motion for the condensate is equivalent to that of charged particles in an electromagnetic field. The vector potential of the electromagnetic field corresponds to the superfluid velocity of the condensate if we set $m\boldsymbol{v}_s = q\boldsymbol{A}$ [27].

For an optically confined BEC, minimization of the energy in Eq. (5) results in a condensate in the SFSS which is lower in energy than the WFSS. We stress that only the SFSS monopole represents a robust ground-state configuration. In order to study a realistic minimum-energy WFSS, we consider a purely magnetic trap provided by the two quadrupole fields in Eq. (1).

We parametrize the magnetic field using polar angles α and β [Fig. 1(c)] such that $\boldsymbol{B}(\boldsymbol{r}) = |\boldsymbol{B}|(\sin\beta\cos\alpha,\ \sin\beta\sin\alpha,\ \cos\beta)^T$. As the Landé g-factor is negative for spin-1 ^{87}Rb and we are considering the WFSS, the hyperfine spin $\boldsymbol{S}$ is antiparallel with the local magnetic field. In the eigenbasis of the spin operator $\hat{F}_z$, the order parameter can be expressed as

$$\begin{pmatrix}\Psi_1\\ \Psi_0\\ \Psi_{-1}\end{pmatrix} = fe^{-i\gamma}\begin{pmatrix}e^{-i\alpha}\sin^2(\beta/2)\\ -\frac{1}{\sqrt{2}}\sin\beta\\ e^{i\alpha}\cos^2(\beta/2)\end{pmatrix} = fe^{-i\gamma}\boldsymbol{\zeta}, \tag{7}$$

where f is the amplitude of the order parameter and $\boldsymbol{\zeta}$ if fixed by Eq. (1). We substitute the order parameter in Eq. (7) into Eq. (3) and denote $\Psi = f_0\boldsymbol{\zeta}$, where $fe^{-i\gamma} = f_0$. This gives a reduced GP equation which can be written in the dimensionless form as

$$-\tfrac{1}{2}[\tilde{\nabla}^2 + 2(\boldsymbol{\zeta}^\dagger\tilde{\nabla}\boldsymbol{\zeta})\cdot\tilde{\nabla} + (\boldsymbol{\zeta}^\dagger\tilde{\nabla}^2\boldsymbol{\zeta})]\tilde{f}_0 + |\tilde{\boldsymbol{B}}|\tilde{f}_0 + (\tilde{c}_0+\tilde{c}_2)\tilde{f}_0^{\,3} = \tilde{\mu}\tilde{f}_0. \tag{8}$$

Here $\tilde{\mu} = \mu/\hbar\omega_r$, $\tilde{\boldsymbol{B}} = \mu_B\boldsymbol{B}/\hbar\omega_r$, $\tilde{f}_0 = a_r^{3/2}f_0$, $\tilde{c}_i = c_iN/(a_r^3\hbar\omega_r)$, and $a_r = \sqrt{\hbar/(m\omega_r)}$. We normalize the complex-valued function $\tilde{f}_0$ to unity as $\int|\tilde{f}_0|^2{\rm d}\tilde{\boldsymbol{r}} = 1$. The minimum-energy density and phase distributions are solved from Eq. (8) using the standard imaginary-time propagation combined with finite-difference methods. The strong-field seeking ground state is found by minimizing the free energy in Eq. (5) with full-spin degrees of freedom using the successive over-relaxation method. The temporal evolution of the monopole defect is solved from the time-dependent GP equation using the split-operator and Crank–Nicolson methods.

III. NUMERICAL RESULTS

The mass of a ^{87}Rb atom is taken to be $m = 1.44\times10^{-25}$kg, the Landé g-factor is $g_F = -1/2$, and the total number of atoms $N = 8\times10^4$. For the coupling constants of ^{87}Rb, we use the value $c_2/c_0 = -0.01$ and adopt $\tilde{c}_0 = 7500$.

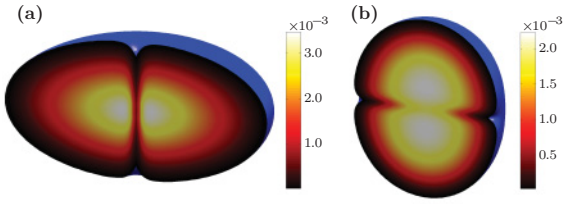

FIG. 2. (Color online) Particle densities corresponding to (a) WFSS and (b) SFSS for $x > 0$. The densities are given in the units of N/a_r^3. The field of view is (a) $8 \times 16 \times 8$ and (b) $6 \times 12 \times 14$ in the units of a_r^3.

For $\omega_r = 2\pi \times 250$Hz, the dimensional values for the parameters are given by $B_1' = 0.1$ T/m for the simulations with the WFSS and $B_1' = -0.03$ T/m with the SFSS. The volume considered in the simulation is $23 \times 23 \times 28$ in the units of a_r^3. The computational grid consists of $141 \times 141 \times 161$ points.

For both SFSS and WFSS, the minimum-energy configuration corresponds to a monopole defect associated with two vortices (Dirac strings), each carrying a single quantum of angular momentum. Both strings carry vorticity toward the monopole defect which lies in the zero point of the magnetic field. In Ref. [20], the Dirac monopole is associated with only one vortex line that carries two quanta of vorticity. For energetic reasons, it is natural that this two-quantum vortex splits into two singly quantized vortices in the ground-state configuration [28,29].

In the WFSS, the Dirac strings lie on the z axis because the magnetic trap is strongest along this direction. For the SFSS, the confinement in the z direction is weaker than in the x and y directions due to the symmetric optical trap, and the two strings lie in the xy plane. For the SFSS, we also consider an asymmetric optical trap of the form $V_{\rm opt}(\boldsymbol{r}) = m(\omega_x^2 x^2 + \omega_y^2 y^2 + \omega_z^2 z^2)/2$. In general, the Dirac strings associated with the monopole defect lie along the direction that minimizes the length of the vortex lines. Particle densities for the SFSS and WFSS are shown in Fig. 2. For the WFSS, the vortices corresponding to the Dirac strings are singular and the particle density vanishes at the vortex core. In the case of the SFSS, particle density is only partially depleted along the two vortices, implying that they are polar-core vortices [30]. The particle densities for each spin state in the WFSS and SFSS are shown in Fig. 3. In the SFSS, the two vortices are manifested as a depletion in the spin density [see Fig. 4(a)].

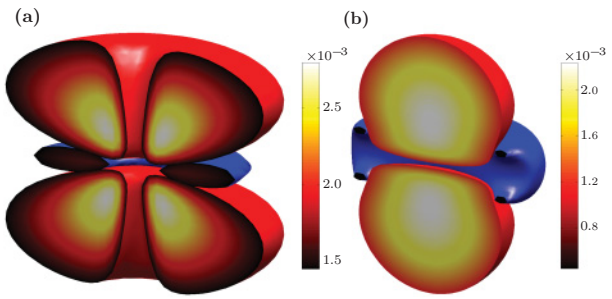

FIG. 3. (Color online) Densities of the three spinor components for (a) WFSS and (b) SFSS. In both panels, the top segment corresponds to $|\Psi_1|^2$, the central segment to $|\Psi_0|^2$, and the bottom segment to $|\Psi_{-1}|^2$. The colorbar scales are in the units of N/a_r^3. The segments are bounded by density isosurfaces for spinor components for $x > 0$. On the plane $x = 0$, the isosurfaces are capped with a density colormap for the corresponding spinor component. In panel (a), all isosurfaces correspond to density $1.4 \times 10^{-3}\ N/a_r^3$ and the singly quantized vortices are manifested as density depletion along the z axis. In panel (b), the vortices lie on the y axis and the isosurfaces correspond to densities $1.2 \times 10^{-3}\ N/a_r^3$ for $|\Psi_1|^2$ and $|\Psi_{-1}|^2$ and $4.5 \times 10^{-4}\ N/a_r^3$ for $|\Psi_0|^2$.

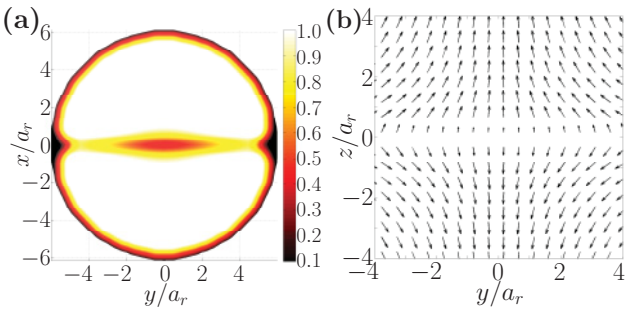

FIG. 4. (Color online) (a) Spin density for the strong-field-seeking ground-state monopole in the $z = 0$ plane. Spin density is depleted along the two vortices, which lie on the y axis. The figure corresponds to spin densities from $0.1 \times 10^{-4}\ N/a_r^3$ to $0.92 \times 10^{-4}\ N/a_r^3$. (b) Spin of the ground-state monopole. The arrows represent the projection of the spin to a plane corresponding to $x = 0$. The S_x component is zero in this plane.

Vorticities and spin textures corresponding to SFSS and WFSS were found to be qualitatively similar, and we present further results only for the SFSS. The condensate spin is shown in Fig. 4(b), and one observes that the spin indeed tends to align with the local magnetic field. From Figs. 5(a)–5(c) we observe

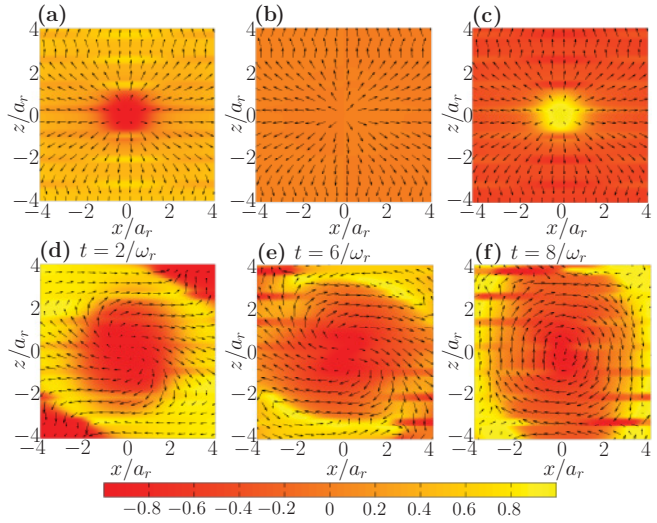

FIG. 5. (Color online) (a)–(c) Vorticity of the ground-state monopole at different locations. (d)–(f) Temporal evolution of vorticity at fixed location. In panels (a)–(c), arrows represent a projection of the unit vorticity $\hat{\Omega}_s = \boldsymbol{\Omega}_s/|\boldsymbol{\Omega}_s|$ to the xz plane for (a) $y = 0.8 \times a_r$, (b) $y = 0 \times a_r$, and (c) $y = -0.8 \times a_r$. In panels (d)–(f), $y = -0.7 \times a_r$ at time instants (d) $t = 2/\omega_r$, (e) $t = 6/\omega_r$, and (f) $t = 8/\omega_r$. The y component is presented with the colormap.

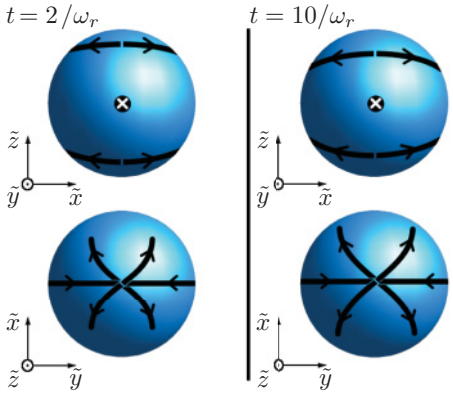

FIG. 6. (Color online) Schematic representation of the temporal evolution of the monopole defect. The spheres represent the atomic cloud and the black lines correspond to vortices. The arrows illustrate the direction of vorticity associated with the single-quantum vortices. The condensate is depicted at two instants of time $t = 2/\omega_r$ and $t = 10/\omega_r$. In the top panels the condensate is viewed along the y axis and in the bottom panels, along the z axis.

that near the monopole defect vorticity takes the hedgehog form of Fig. 1(b).

Next we study the dynamics of the monopole after the external magnetic fields are turned off. We take the initial state to be the strong-field-seeking ground state with vortices on the y axis. The fields are turned off instantaneously and the state is evolved up to $10/\omega_r$ with a time step $10^{-4}/\omega_r$. During the time evolution, the Dirac strings are observed to expand, see Figs. 5(d)–5(f). Furthermore, two antimonopoles emerge from the boundary of the condensate and move toward the center of the trap. The emergent antimonopoles are characterized by Dirac strings that carry vorticity outward from the monopole. Similarly to the ground-state monopole, the Dirac strings are coreless vortices. We note that the Dirac strings associated with antimonopoles guarantee that the total vorticity remains zero after the antimonopoles emerge. A schematic representation of the temporal evolution is shown in Fig. 6, and high-resolution figures of the simulation are available in the supporting online material [31]. At the end of the simulation, the vorticity of the monopole defect has spread out and is no longer strictly of the hedgehog form.

In conclusion, we have shown that a monopole defect may exist as the ground state of a dilute ferromagnetic spin-1 BEC in the presence of an experimentally feasible magnetic field configuration. Vorticity of this defect is analogous to the magnetic field of a magnetic monopole. The ground-state monopole is associated with two Dirac strings that extend symmetrically outward from the monopole defect. From the relation between the geometric charge of the monopole defect and the total vorticity in the system, it follows that each of the two coreless vortices associated with the SFSS monopole defect carry a single quantum of angular momentum. This is remarkable, since in general the angular momentum associated with coreless vortices is not quantized. Thus, the monopole defect is responsible for the quantization of coreless vortices similarly to the Dirac magnetic monopole, which imposes the quantization of electric charge. If monopoles are to appear spontaneously in BECs, one would expect for energetic reasons that they are associated with two singly quantized vortices instead of a single two-quantum vortex. Hence such monopoles are of great interest. In the experiments, the ground-state monopole can be created during the cooling process, without the need to adjust the external magnetic fields in time. These monopoles are expected to be extremely robust and long lived.

ACKNOWLEDGMENTS

We acknowledge the Emil Aaltonen Foundation, the Academy of Finland, Finnish Graduate School in Computational Sciences, The Research Foundation of Helsinki University of Technology, and Harvard–MIT CUA for financial support, and the Center for Scientific Computing, Finland, for computing resources.

[1] J. M. Kosterlitz and D. J. Thouless, J. Phys. C **5**, L124 (1972).
[2] T. W. B. Kibble, J. Phys. A **9**, 1387 (1976).
[3] P. A. M. Dirac, Proc. R. Soc. London Sect. A **133**, 60 (1931).
[4] T. H. R. Skyrme, Proc. R. Soc. London Sect. A **260**, 127 (1961).
[5] P. Langacker and S.-Y. Pi, Phys. Rev. Lett. **45**, 1 (1980).
[6] J. P. Preskill, Phys. Rev. Lett. **43**, 1365 (1979).
[7] A. E. Leanhardt, Y. Shin, D. Kielpinski, D. E. Pritchard, and W. Ketterle, Phys. Rev. Lett. **90**, 140403 (2003).
[8] L. S. Leslie, A. Hansen, K. C. Wright, B. M. Deutsch, and N. P. Bigelow, Phys. Rev. Lett. **103**, 250401 (2009).
[9] Y. Kawaguchi, M. Nitta, and M. Ueda, Phys. Rev. Lett. **100**, 180403 (2008).
[10] C. M. Savage and J. Ruostekoski, Phys. Rev. Lett. **91**, 010403 (2003).
[11] C. M. Savage and J. Ruostekoski, Phys. Rev. A **68**, 043604 (2003).
[12] H. Zhai, W. Q. Chen, Z. Xu, and L. Chang, Phys. Rev. A **68**, 043602 (2003).
[13] H. T. C. Stoof, E. Vliegen, and U. Al Khawaja, Phys. Rev. Lett. **87**, 120407 (2001).
[14] V. Pietilä and M. Möttönen, Phys. Rev. Lett. **102**, 080403 (2009).
[15] M. Nakahara, *Geometry, Topology and Physics* (IOP Publishing, Ltd., Bristol, 1990).
[16] T. Isoshima, M. Nakahara, T. Ohmi, and K. Machida, Phys. Rev. A **61**, 063610 (2000).
[17] S.-I. Ogawa, M. Möttönen, M. Nakahara, T. Ohmi, and H. Shimada, Phys. Rev. A **66**, 013617 (2002).
[18] J.-P. Martikainen, A. Collin, and K.-A. Suominen, Phys. Rev. Lett. **88**, 090404 (2002).
[19] J. Choi, W. J. Kwon, and Y. Shin, e-print arXiv:1110.3858.
[20] V. Pietilä and M. Möttönen, Phys. Rev. Lett. **103**, 030401 (2009).

[21] A. Auerbach, *Interacting Electrons and Quantum Magnetism* (Springer, New York, 1994), pp. 104–105.
[22] N. N. Klausen, J. L. Bohn, and C. H. Greene, Phys. Rev. A **64**, 053602 (2001).
[23] M. Ueda, *Fundamentals and New Frontiers of Bose-Einstein Condensation* (World Scientific Publishing Company, Inc., 2010).
[24] N. D. Mermin and T.-L. Ho, Phys. Rev. Lett. **36**, 594 (1976).
[25] T.-L. Ho, Phys. Rev. Lett. **81**, 742 (1998).
[26] T. Ohmi and K. Machida, J. Phys. Soc. Jpn. **67**, 1822 (1998).
[27] T. L. Ho and V. B. Shenoy, Phys. Rev. Lett. **77**, 2595 (1996).
[28] J. A. M. Huhtamäki, M. Möttönen, T. Isoshima, V. Pietilä, and S. M. M. Virtanen, Phys. Rev. Lett. **97**, 110406 (2006).
[29] Y. Shin, M. Saba, M. Vengalattore, T. A. Pasquini, C. Sanner, A. E. Leanhardt, M. Prentiss, D. E. Pritchard, and W. Ketterle, Phys. Rev. Lett. **93**, 160406 (2004).
[30] T. Isoshima, K. Machida, and T. Ohmi, J. Phys. Soc. Jpn. **70**, 1604 (2001).
[31] See Supplemental Material at http://link.aps.org/supplemental/10.1103/PhysRevA.84.063627 for high-resolution figures.